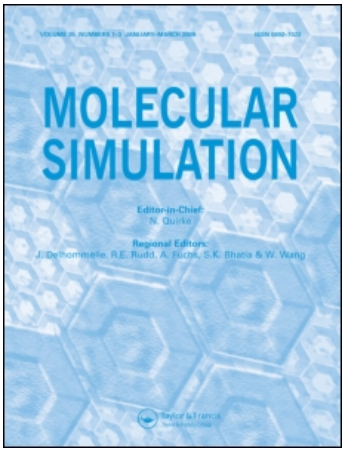

Molecular Simulation
Publication details, including instructions for authors and subscription information:
http://www.informaworld.com/smpp/title~content=t713644482

Molecular Dynamics Simulation Studies of the Density and Temperature Dependence of Self-diffusion in a Cylindrical Micropore

T. Demi[a]; D. Nicholson[b]
[a] Institute of Cancer Research, Royal Cancer Hospital, Sutton, Surrey [b] Department of Chemistry, Imperial College of Science, Technology and Medicine, University of London, London

To cite this Article Demi, T. and Nicholson, D.(1991) 'Molecular Dynamics Simulation Studies of the Density and Temperature Dependence of Self-diffusion in a Cylindrical Micropore', Molecular Simulation, 5: 6, 363 — 381
To link to this Article: DOI: 10.1080/08927029108022422
URL: http://dx.doi.org/10.1080/08927029108022422

Molecular Simulation, 1991, Vol. 5, pp. 363–381
Reprints available directly from the publisher
Photocopying permitted by license only

MOLECULAR DYNAMICS SIMULATION STUDIES OF THE DENSITY AND TEMPERATURE DEPENDENCE OF SELF-DIFFUSION IN A CYLINDRICAL MICROPORE

T. DEMI

Institute of Cancer Research, Royal Cancer Hospital, Clifton Avenue, Sutton, Surrey SM2 5PX

D. NICHOLSON*

Department of Chemistry, Imperial College of Science, Technology and Medicine, University of London, London, SW7 2AY

(*Received December 1989, accepted March 1990*)

We report Molecular Dynamics calculations of radial density profiles and self-diffusion coefficients of Lennard-Jones fluids in a cylindrical pore of radius 2σ, for a wide range of temperatures and densities. At $n_p\sigma^3 = 0.825$ the self-diffusion coefficient parallel to the pore walls $D_\parallel^*$ follows a monotonic (nearly linear) increase with kT/ε and is very similar to that of the bulk self-diffusion coefficient D_b^*. At $n_p\sigma^3 = 0.4$ and $kT/\varepsilon \leqslant 1.0$ the curve of $D_\parallel^*$ vs. kT/ε shows a distinct inflection in the region $0.7 \leqslant kT/\varepsilon \leqslant 0.9$ and values of $D_\parallel^*$ are much less than D_b^* decreasing to near solid state values at very low temperatures. At the highest temperature studied, $kT/\varepsilon = 2.98$, $D_\parallel^*$ is almost inversely proportional to density and in a fairly close agreement with that of D_b^*. At $KT/\varepsilon = 0.49$, $D_\parallel^*$ is much smaller than D_b^*. The motion of adsorbate particles normal to the walls is also discussed.

KEY WORDS: Diffusion, cylindrical pores, molecular dynamics

INTRODUCTION

Much interest has been shown in recent years in the structure and equilibrium properties of fluids confined in the micropore size range. Although in the most realistic situations the internal structure of the pore is complicated, model idealizations have been employed in theoretical studies. These are intended to throw light on the understanding of the molecular phenomena underlying experimental observations. The most widely studied geometries so far are the slit [1,2,3,4] and cylindrical [5,6,7,8,9,10,11] models. Both Monte Carlo (MC) and Molecular Dynamics (MD) computer simulation techniques have been extensively applied to the study of fluids in narrow pores of different geometries. More than 20 years ago Rahman applied the Molecular Dynamics technique to simulate bulk liquid argon [12]. An important observation from his results, which agreed reasonably well with experimental work, was the appearance of a large negative minimum in the velocity auto-correlation function (VACF). This observation was later confirmed by Alder and his group

*Author to whom correspondence should be addressed.

[13,14,15] for hard sphere fluids and also by Levesque and Verlet [16] for Lennard-Jones fluids. The former authors were able to explain the phenomenon in terms of hydrodynamics [14]. The adsorption behaviour of hard sphere fluids near a hard wall has also been investigated by several authors [17,18,19,20]. Self-diffusion coefficients of hard sphere and Lennard-Jones fluids between two adsorbing parallel walls have been studied by Subramanian and Davis [2], Antonchenko and others [1], and Magda, Tirrell and Davis [3] who calculated the self-diffusion coefficient for different pore sizes and found that it oscillated with pore width. A break in the slope of the mean square displacement (MSD) was also observed in this work and was found to coincide approximately with the time at the negative backscattering minimum in the VACF. This was explained as in reference [14], in terms of sound-waves that reflect off the pore walls and return to backscatter the particles at a later time thereby creating a large negative minimum in the VACF and a break in the slope of the MSD. Hindered diffusion of hard sphere fluids in cylindrical pores has been investigated by Suh and McElroy [9], using the MD technique. Two particle/pore wall conditions were investigated: specular and diffuse reflection. The authors confirmed the soundwave hypothesis of Magda, Tirrell and Davis [3]. The adsorption of Lennard-Jones molecules in spherical model zeolite cavities has recently been studied by Woods *et al.* [21]. Good agreement was observed between Grand Canonical Monte Carlo (GCMC) results and those obtained from the direct calculation of the partition functions.

In the present paper we have investigated the adsorption and diffusion behaviour of Lennard-Jones fluids in structureless cylindrical pores using molecular dynamics. Results were obtained over a wide range of temperatures and densities and include density profiles, temperature and density dependence of the velocity auto-correlation function (VACF) and of the mean square displacement (MSD) and self-diffusion coefficients parallel and perpendicular to the pore walls. All the reported results were found to be in qualitative agreement with previous related work [3,9,11].

2. METHOD

The system studied was used to approximate fluid krypton in a cylindrical pore modelled as a structureless rigid wall. The Lennard-Jones (6, 12) potential

$$v^{LJ}(r) = 4\varepsilon\left[\left(\frac{\sigma}{r}\right)^{12} - \left(\frac{\sigma}{r}\right)^{6}\right] \tag{1}$$

with a cut-off distance of $r_c = 3.5\sigma$ and σ and ε given from Table 1, was used to model the fluid-fluid interactions. The external field represents the fluid-solid interactions which were approximated by an average over the uniformly distributed atoms in the solid,

$$v_{1s}(r_i) = \rho_s \int_s v_{ij}(r_i, r_j)\, dr_j \tag{2}$$

where ρ_s is the solid density and $v_{ij}(r_i, r_j)$ is the Lennard-Jones potential given by

Table 1 Hard sphere and Lennard-Jones parameters for krypton-krypton interaction

σ, collision diameter/nm	0.357
ε/k, Energy parameter/K	201.9

Table 2 Molecular parameters for the interaction between krypton and the MS-13X cavity walls

σ_{1s}, Gas-Solid collision diameter/nm	0.3165
$\rho_s \varepsilon_{1s}/k$, Energy parameter/Knm^{-2}	1315

equation (1). The parameters were those used by Soto and Myers [22] for the interaction of krypton with zeolitic oxygen (Table 2). The external field was tabulated at intervals of 0.01σ and a linear interpolation method was used to interpolate between tabulated points. The numerical equations of motions were solved using Verlet's Leap Frog algorithm [23,24] with a time step of 2.5×10^{-3}ps. Periodic boundary conditions were employed only in the z direction (taken along the pore axis). The starting configuration was formed by placing annular monolayers of atoms perpendicular to the axis of the cylinder of radius R, measured from the centre of the pore to the centre of a wall atom. The distance between the layers was chosen to give a prescribed overall density within the volume bounded by $(R - \sigma/2)$. The initial velocities of the particles were randomly chosen from the Maxwell-Boltzmann distribution. Most of the MD simulations were performed in cylindrical pores of radius 2σ and one simulation was performed in a 5σ pore. The number of time steps used in the production runs of the simulations was between 30000–150000 depending on the radius of the pore, the temperature and density of the system. A post-simulation calculation [25] was used for the calculation of the VACF and the MSD. All simulations were performed on the CRAY-1s at ULCC.

3. RESULTS AND DISCUSSION

3.1 Density profiles

Radial density profiles were produced by dividing the pore into annular bins, each having a radial length of 0.01σ. The density was calculated in each bin by counting the number of particles in the bin and dividing its volume,

$$\rho_{r_i} = \frac{\langle N_i \rangle}{\pi[(r_i + \Delta r/2)^2 - (r_i - \Delta r/2)^2]L} \tag{3}$$

where r_i denotes the radial coordinate at the center of the ith bin and L the axial length. The $\langle ... \rangle$ in the numerator indicate a time average of N_i, the number of particles in the ith bin. Figures 1 and 2 show the local density profiles in a temperature range kT/ε, 0.25 – 2.98 for the average pore density $n_p\sigma^3 = 0.825$ and 0.62 – 3.48 for $n_p\sigma^3 = 0.4$. One can see from both figures that when the temperature decreases the fluid becomes more structured, in agreement with the results of Panagiotopoulos [10]. The peak near to the pore walls is approximately Gaussian at $kT/\varepsilon = 0.25$ and slightly skewed at 2.98. It is also shifted towards the pore walls with increasing temperature. This can be attributed to the fact that at high temperatures the particles have enough energy to overcome the highly repulsive field near the pore walls and to move closer to them. In Figures 3 and 4 we present the local density profiles in an average pore density range $n_p\sigma^3 = 0.825$–0.2 at $kT/\varepsilon = 0.49$ and 2.98 respectively. At the lower temperature of $kT/\varepsilon = 0.49$, highly localized behaviour is observed. The peak at the centre of the pore is higher than the peak at the wall at all densities. At $kT/\varepsilon = 2.98$, and $n_p\sigma^3 \leqslant 0.3$, only the adsorption peak due to the pore walls is

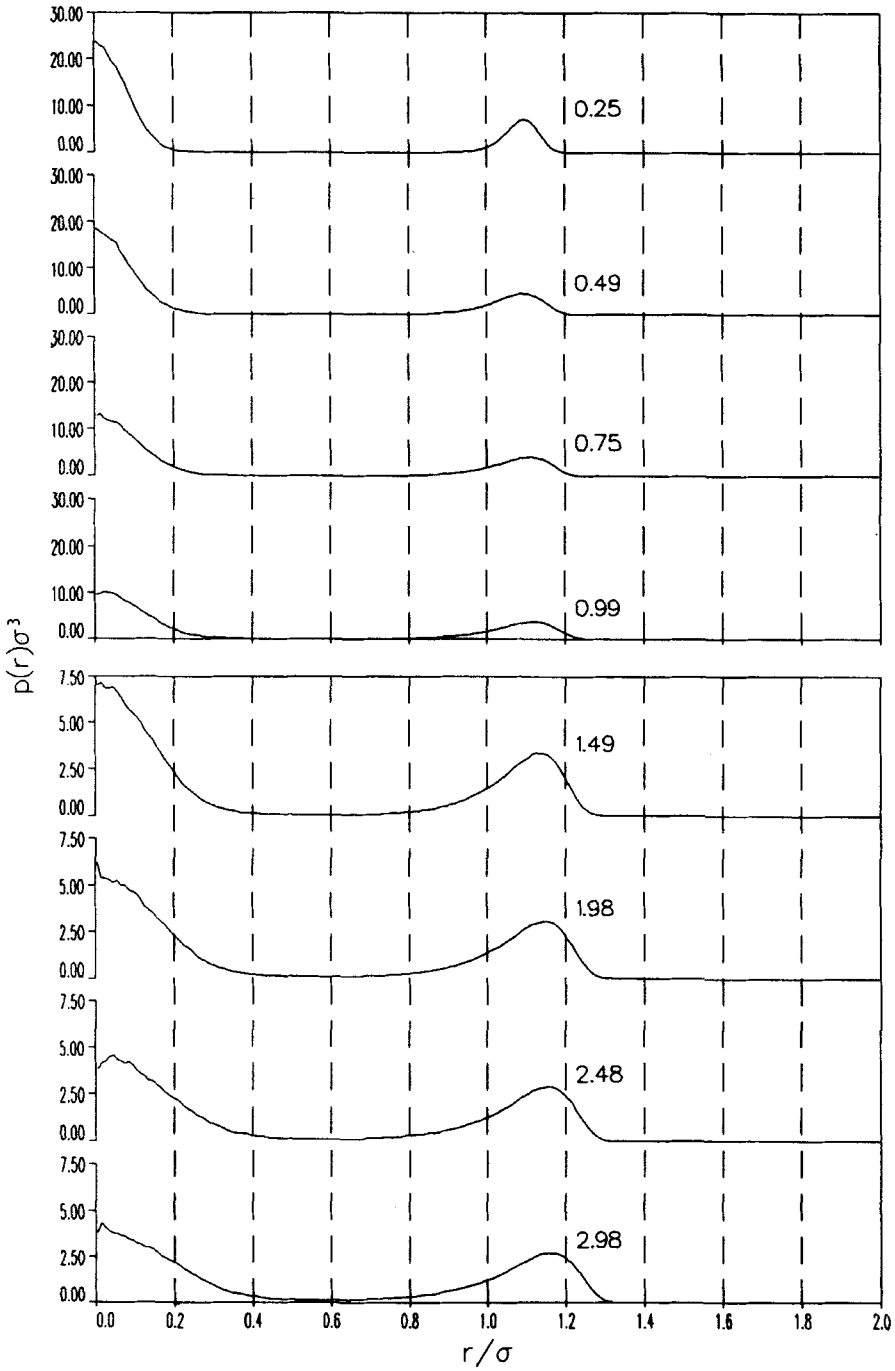

Figure 1 Density profiles in a cylindrical pore of radius 2σ, for a series of temperatures. The results were obtained from MD data at $n_p\sigma^3 = 0.825$. The number on the right of the peak indicates the temperature kT/ε.

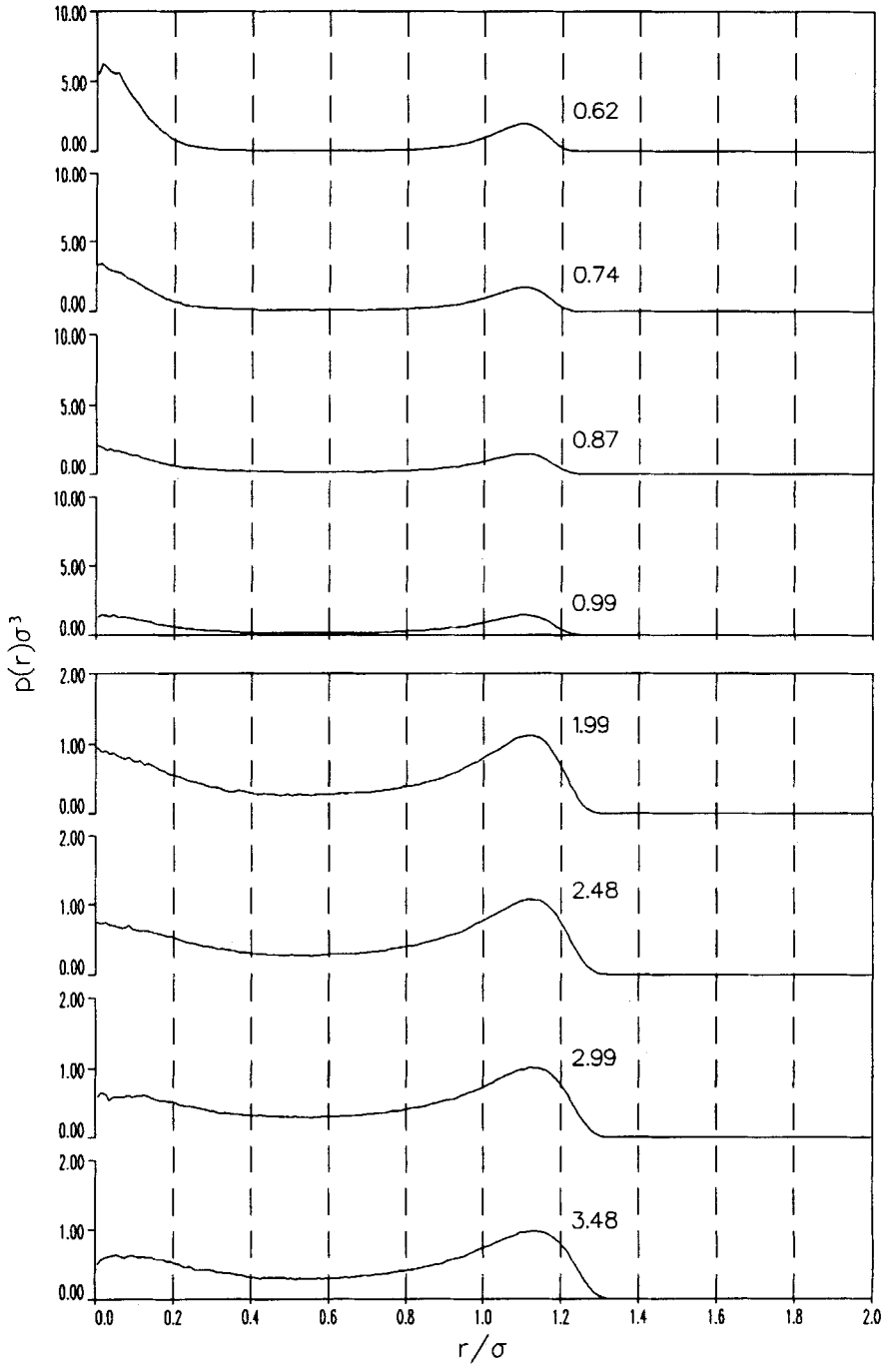

Figure 2 As for Figure 1 at density $n_p\sigma^3 = 0.4$.

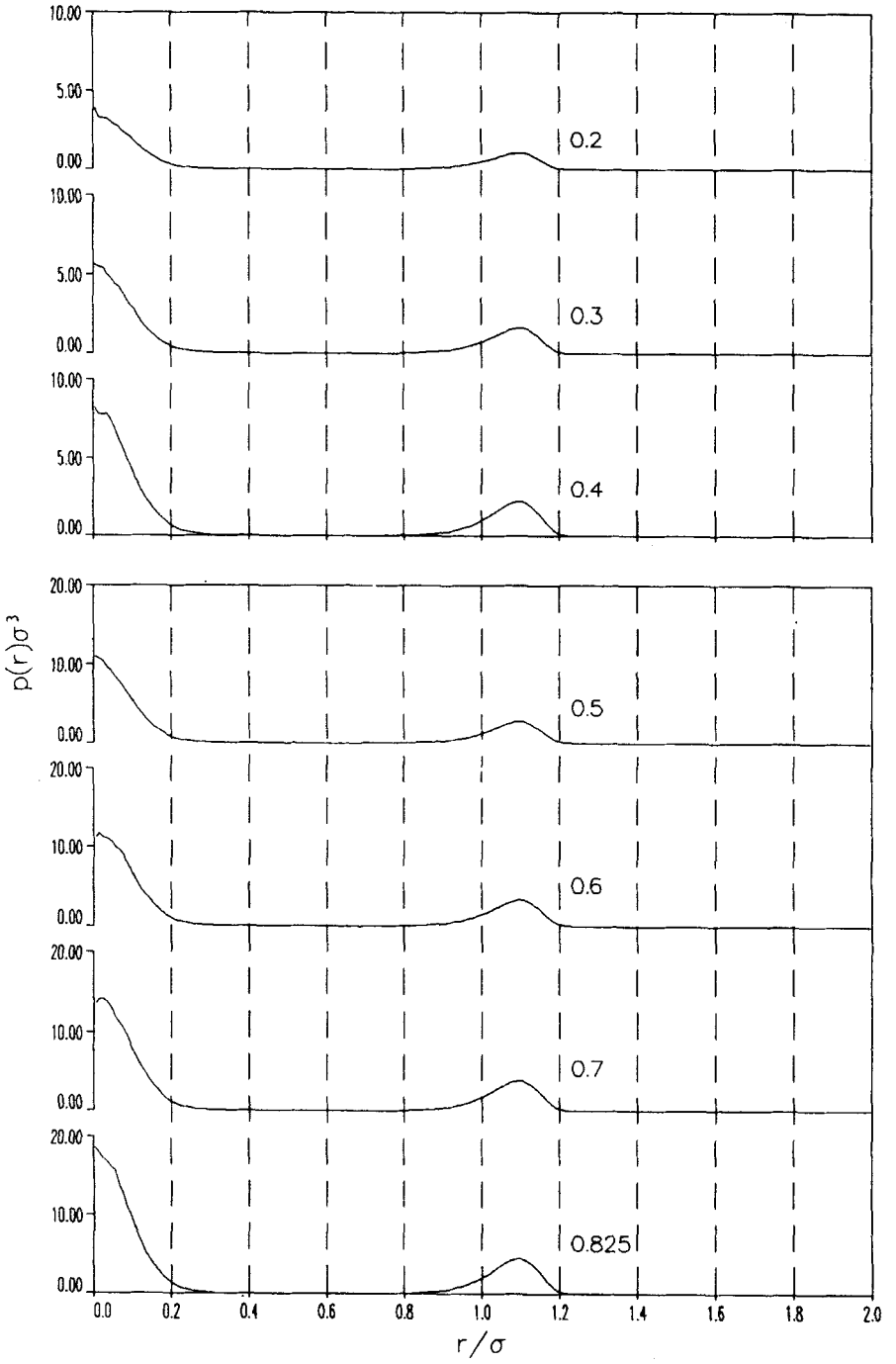

Figure 3 Density profiles in a cylindrical pore of radius 2σ, for a series of densities. The results were obtained from MD data at $kT/\varepsilon = 0.49$. The number on the right of the peak indicates the density $n_p\sigma^3$.

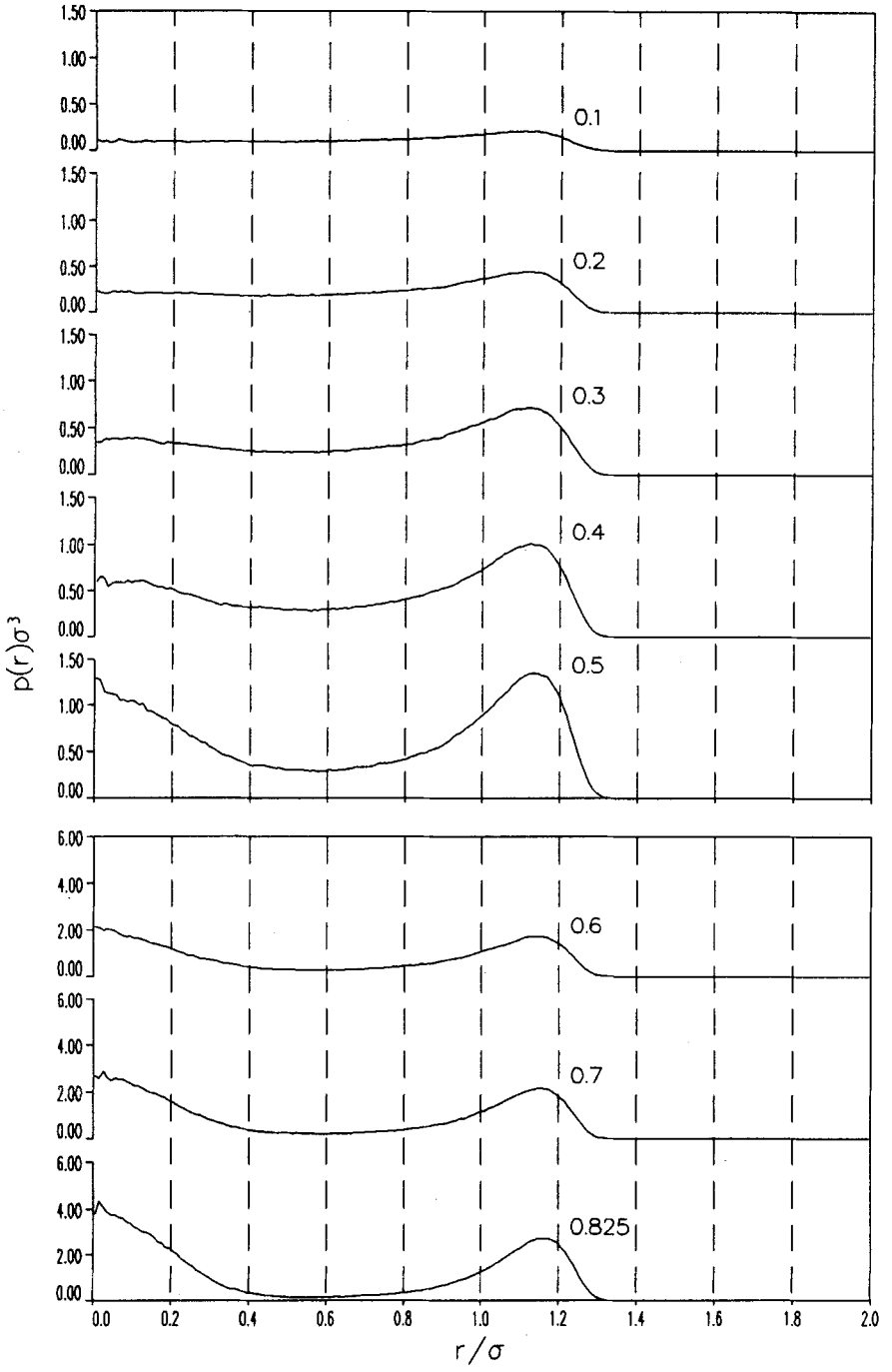

Figure 4 As for Figure 3 at $kT/\varepsilon = 2.98$.

present. As the density increases, however, a peak at the center of the pore gradually emerges, and at $n_p\sigma^3 \geqslant 0.6$, it is higher than the peak at the wall. These observations are in agreement with the results of Woods *et al.* [21]. Figures 5 and 6 show the trajectories of the particles in the simulation box of radius 2σ and length 24σ, as a projection in the z,t plane, at density $n_p\sigma^3 = 0.825$ and temperature $kT/\varepsilon = 2.98$ and 0.49 respectively. At $kT/\varepsilon = 0.49$ the fluid appears to be solid-like with the particles oscillating around their initial positions.

3.2 Self-Diffusion Coefficients

The macroscopic quantity which characterizes all diffusion processes in a one-component fluid is the self-diffusion coefficient D. The components of D parallel $D_\parallel^*$ and perpendicular $D_\perp^*$ to the pore walls were calculated both from the numerical integration of the velocity auto-correlation function (VACF), and from the slope of the mean square displacement of the particles (MSD). In the former (VACF),

$$D = \int_0^\infty \left[1/N \sum_{i=1}^{N} \langle v_{iz}(t)\, v_{iz}(0) \rangle \right] \tag{4}$$

$$D_\perp = 1/2 \int_0^\infty \left[1/N \sum_{i=1}^{N} (\langle v_{ix}(t)\, v_{ix}(0) \rangle + \langle v_{iy}(t)\, v_{iy}(0) \rangle) \right] \tag{5}$$

where v_{iv}, denotes the v'th component of the velocity of particle i at time t, and N is the number of particles in the simulation box, $\langle ... \rangle$ indicate that the quantity $(v(t)_{iv} v(0)_{iv})$ was calculated for all particles in the simulation box. From the mean-square displacement (MSD)

$$D = \lim_{t \to \infty} 1/N \sum_{i=1}^{N} (1/2t)\, (\langle (Z_i(t) - Z_i(0))^2 \rangle) \tag{6}$$

$$D_\perp = \lim_{t \to \infty} 1/N \left[\sum_{i=1}^{N} (1/4t)\, (\langle (X_i(t) - X_i(0))^2 \rangle + \langle (Y_i(t) - Y_i(0))^2 \rangle) \right] \tag{7}$$

where $X(t)$, $Y_i(t)$, $Z_i(t)$ are the components of the position vectors of particle i in the x,y and z directions, at time t, and $X_i(0)$, $Y_i(0)$ and $Z_i(0)$ are the position vectors of the same particle i in the three directions at time origin 0.

$D_\perp^*$ reflects the constraint on molecules moving normal to the pore walls. Since this motion is bounded, $D_\perp^*$ would be zero in the limit $t \to \infty$. At finite times the MSD and VACF are nevertheless useful as an indicator of the extent to which the molecules are localized. At low temperatures ($kT \ll \varepsilon_{ls}$) adsorbate atoms near to the wall will vibrate normal to the surface with a frequency $\approx 10^{12} s^{-1}$, and $D_\perp$ will then $\to 0$ in $\approx 10^3$ time steps. The constraints imposed by other molecules however will also play a part; high densities would be expected to favour localization. Likewise pore size will modify the MSD at short and intermediate times.

3.2.1 Pore radius dependence of D

The self-diffusion coefficients parallel D^* and perpendicular $D_\perp^*$ to the pore walls reduced by $\sigma(\varepsilon/m)^{1/2}$ have been calculated for both the pore radii studied (2σ and 5σ), at $kT/\varepsilon = 1.49$ and $n_p\sigma^3 = 0.4$. In Table 3 we present the values of $D_\parallel^*$ and $D_\perp^*$, from VACF and MSD data for these two pore radii. Here the finite time diffusion coefficients D^* and $D_\perp^*$ have been measured by taking slopes from the MSD curves in the

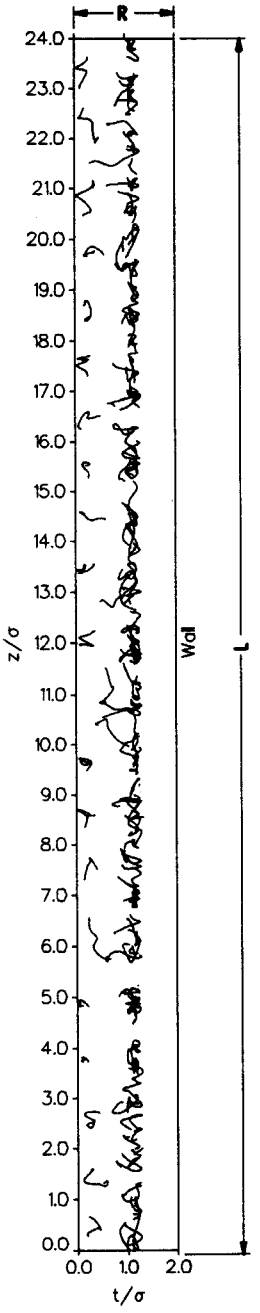

Figure 5 Trajectories of particles for a fluid in a cylindrical simulation box of radius $R = 2\sigma$ and a length $L = 24\sigma$, as a projection onto a radial (z,t) plane. The temperature $kT/\varepsilon = 2.98$ and the density $n_p\sigma^3 = 0.825$. The trajectories of the particles were recorded at each time step over approximately 100 time steps of the simulation.

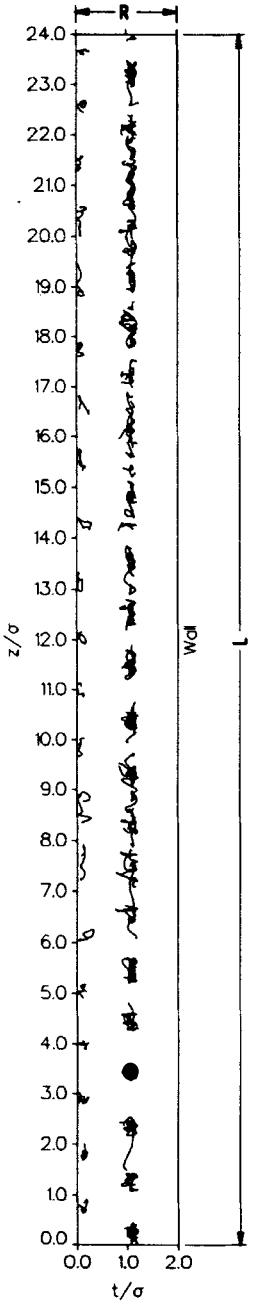

Figure 6 As for Figure 5 at $kT/\varepsilon = 0.49$.

Table 3 Self-diffusion coefficient parallel $D_{\parallel}^*$ and perpendicular $D_{\perp}^*$ to the pore walls in units of $\sigma(\varepsilon/m)^{1/2}$, calculated from VACF and MSD data, in cylindrical pores of radius 2σ and 5σ. The last column presents the bulk self-diffusion coefficient calculated from equation (8). The temperature is $kT/\varepsilon = 1.49$ and the density $n_p\sigma^3 = 0.4$

R/σ	*Range/(ps)*†	$D_{\parallel}^{*\ddagger}$	$D_{\parallel}^{*\S}$	*Range/(ps)*¶	$D_{\perp}^{*\ddagger}$	$D_{\perp}^{*\S}$	D_b^*
2.0	2.50–4.49	0.441	0.425	3–4.49	0.130	0.177	0.429
5.0	2.00–4.49	0.410	0.423	1–4.49	0.308	0.314	0.429

†Time interval in ps from which the MSD parallel to the pore walls is estimated
‡From MSD data
§From VACF data
¶Time interval in ps from which the MSD perpendicular to the pore walls is estimated

range stated in the table, as well as from the numerical integration of the VACFS. For these timescales, the numbers given may be regarded as an index of the relative mobility in the two pores under comparable conditions of temperature and density which would account for the larger value of $D_{\perp}^*$ in the 5σ pore where a greater density gradient exists between the pore wall and the axis. The value of the reduced bulk diffusion coefficient in a Lennard-Jones fluid was calculated from [26]

$$D_b^* = a + bT^{*i} + \rho^{*j}(c + dT^{*k}) + \rho^{*l}(e + fT^{*m}) + \rho^{*n}(g + hT^{*0}) \quad (8)$$

$D_{\parallel}^*$ was found to be the same for both pores within the uncertainty of the calculations and very close to the bulk value D_b^* (Table 3).

3.2.2 *Temperature dependence*

The temperature dependence of $D_{\parallel}^*$ was studied in a cylindrical pore of radius 2σ for two densities, $n_p\sigma^3 = 0.825$ and 0.4. In Tables 4 and 5 we present the values of $D_{\parallel}^*$ calculated from VACF and MSD data for these densities and for a series of temperatures. The agreement between the values of $D_{\parallel}^*$ from VACF and MSD data at both densities is satisfactory. Figures 7 and 8 show the temperature dependence of $D_{\parallel}^*$ calculated from MSD data and D_b^* from equation (8) for $n_p\sigma^3 = 0.825$ and 0.4 respectively. At $n_p\sigma^3 = 0.825$, $D_{\parallel}^*$ follows a monotonic (nearly linear) increase with T very close to that of D_b^*. The agreement is fairly close over the whole of the temperature range, although the ratio $D_b^*/D_{\parallel}^*$ approaches unity more closely as kT/ε increases. The consistently higher values of $D_{\parallel}^*$ indicate that there is a greater fluidity

Table 4 $D_{\parallel}^*$ calculated from MSD and VACF data at different temperatures in a cylindrical pore of radius 2σ. The density is $n_p\sigma^3 = 0.825$. The last column presents the bulk self-diffusion coefficient D_b^*, calculated from equation (8).

kT/ε	*Range/(ps)*†	$D_{\parallel}^{*\ddagger}$	$D_{\parallel}^{*\S}$	D_b^*
0.25		0.0000	0.0008	
0.49	2.50–4.49	0.025	0.028	0.015
0.99	1.50–4.49	0.071	0.072	0.060
1.49	3.00–4.49	0.109	0.116	0.099
1.98	3.00–4.49	0.147	0.156	0.134
2.48	3.00–4.49	0.177	0.177	0.169
2.98	3.00–4.49	0.218	0.218	0.202

†Time interval in ps from which the MSD parallel to the pore walls is estimated
‡From MSD data
§From VACF data

Table 5 $D_{\parallel}^{*}$ calculated from MSD and VACF data at different temperatures. The density is $n_p\sigma^3 = 0.4\sigma$. The last column presents the bulk self-diffusion coefficient D_b^{*} calculated from equation (8).

kT/ε	*Range/(ps)*†	$D_{\parallel}^{*}$‡	$D_{\parallel}^{*}$§	D_b^{*}
0.25		0.000	0.001	
0.49	2.00–4.49	0.044	0.044	0.108
0.62	3.00–4.49	0.094	0.094	0.166
0.74	3.00–4.49	0.213	0.212	0.212
0.87	3.00–4.49	0.296	0.298	0.257
0.99	3.00–4.49	0.328	0.327	0.295
1.49	3.00–4.49	0.452	0.425	0.429
1.98	3.00–4.49	0.572	0.573	0.536
2.48	2.00–4.49	0.684	0.695	0.631
2.98	2.50–4.49	0.748	0.746	0.716
3.48	2.30–4.49	0.804	0.823	0.793

†Time interval in ps from which the MSD parallel to the pore walls is estimated
‡From MSD data
§From VACF data

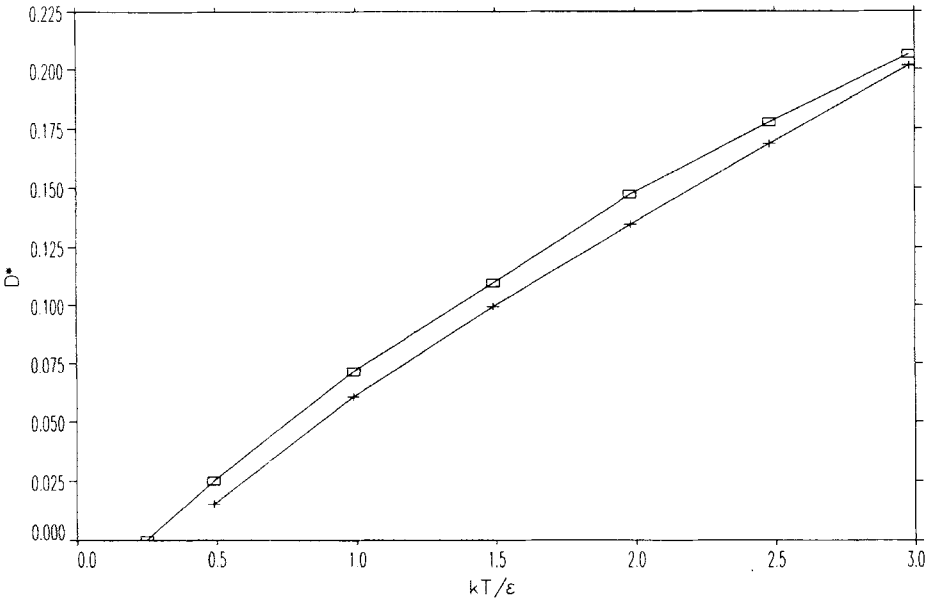

Figure 7 Self-diffusion coefficient parallel $D_{\parallel}^{*}$ (□) to the pore of radius 2σ as a function of temperature. Values were calculated from MSD data. Also shown is the bulk self-diffusion coefficient D_b^{*} (+) calculated from equation (8). The density is $n_p\sigma^3 = 0.825$.

in the pore than in the bulk. At $n_p\sigma^3 = 0.4$, the curve of $D_{\parallel}^{*}$ vs. kT/ε shows a distinct inflection in the region $0.7 \leqslant kT/\varepsilon \leqslant 0.9$ and values are much less than D_b^{*}, decreasing to solid state or near solid state values ($D_{\parallel}^{*} = 0$) at very low temperatures. This suggests that a transition occurs in this region which is centered at $kT/\varepsilon \sim 0.75$. These observations are consistent with the density profiles in Figures 1 ($n_p\sigma^3 = 0.825$) and 2($n_p\sigma^3 = 0.4$). At $n_p\sigma^3 = 0.4$ and $kT/\varepsilon \leqslant 0.74$, the adsorbate is strongly localized

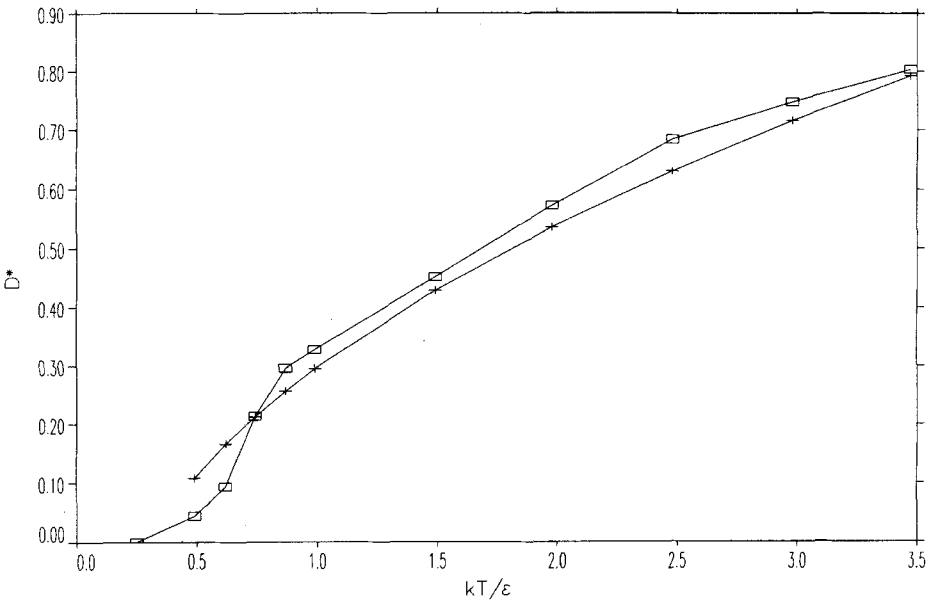

Figure 8 As Figure 7 at density $n_p\sigma^3 = 0.4$.

into layers and the local density is zero in the region between the maxima. At $kT/\varepsilon = 0.74$ the minimum in the density profile rises above zero showing that there is now a finite probability of finding molecules in this intermediate region. At the higher density on the other hand (see Figure 1) the local density is zero at its minimum for all temperatures. Figures 9, 10a and 10b show the MSD and VACF for motion normal to the pore walls and at different temperatures. The slope of these MSD curves does not remain constant but gradually decreases, tending to zero at long times (Figure 9). This effect is seen more clearly as temperature increases, in keeping with the expectation that the velocity of the particles is proportional to $T^{1/2}$. At low temperatures when the adsorbate molecules are likely to be localized vibrators, the wall effect is seen in the minimum in the VACF curves; as temperature increases this minimum disappears and the VACF curves change character, developing an increasingly pronounced long time tail. This suggests that at these higher temperatures a vortex flow pattern develops [14], originating from interaction between particles moving in a direction opposite to the initial direction of the diffusing particle, due to its reflection off the pore walls. The transition at $kT/\varepsilon \approx 0.75$ mentioned above is also apparent in the change in character of these VACF curves.

3.2.3 Density dependence of D

Tables 6 and 7 present the values of $D_\parallel^*$ and D_b^* at $kT/\varepsilon = 2.98$ and $kT/\varepsilon = 0.49$ respectively. In Figures 11 and 12, $D_\parallel^*$ and, D_b^* are plotted against density at $kT/\varepsilon = 2.98$ and 0.49 respectively. At $kT/\varepsilon = 2.98$, $D_\parallel^*$ is proportional to $(density)^{-0.85}$ compared with the $(density)^{-0.72}$ calculated from equation (8) and the $(density)^{-2}$ proportionality observed for bulk fluid by Verlet [16]. $D_\parallel^*$ is also very close to the bulk value D_b^* at moderate to high densities and only at $n_p\sigma^3 \leqslant 0.3$ is deviation observed. It is surprising that $D_\parallel^*$ is lower than the bulk diffusion coefficient at these low

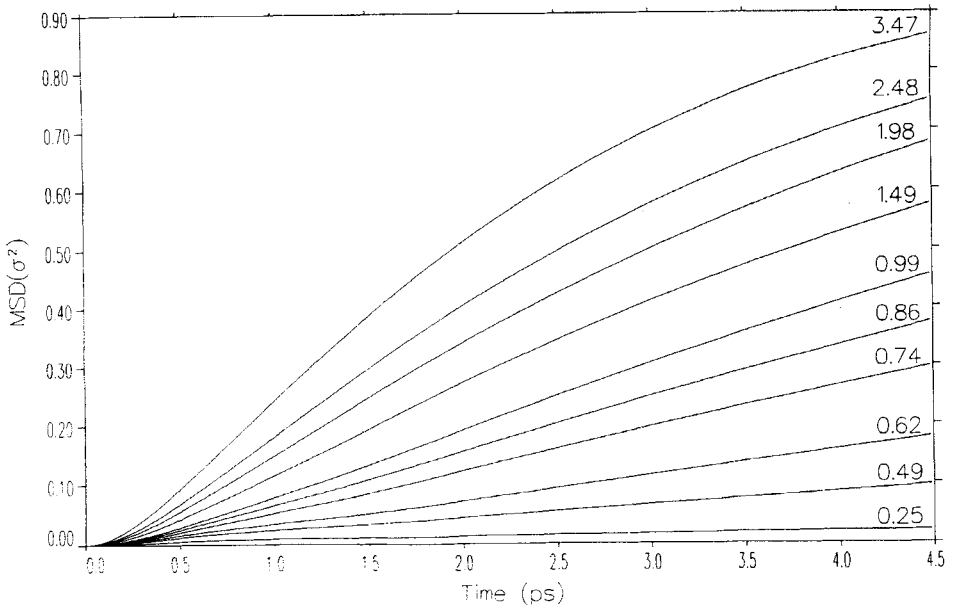

Figure 9 Mean square displacement perpendicular to the pore walls in a cylindrical pore of radius 2σ, at $n_p\sigma^3 = 0.4$ for a series of temperatures.

densities, since it would be expected that the increase in $D_\parallel^*$ due to the availability of larger diffusion paths in the less dense region of the non-uniform fluid (compare Figures 3 and 4) would more than compensate for the decrease in the dense region near the wall. However it is the low density regions which are the more sensitive to long time tail effects in the VACF (and corresponding effects in the MSD). The observed results at low densities are therefore probably best regarded with caution because of the inaccuracies introduced in the numerical integration of the VACF. Figure 13 demonstrates that the contributions to the VACF appearing at a later time than that examined (4ps) are much more significant here. It seems probable that an

Table 6 $D_\parallel^*$ calculated from MSD and VACF data for different densities in a cylindrical pore of radius 2σ. The temperature is $kT/\varepsilon = 2.98$. The bulk self-diffusion coefficient D_b^* calculated from equation (8) is also presented.

$n_p\sigma^3$	*Range/(ps)*[†]	$D_\parallel^{*\ddagger}$	$D_\parallel^{*\S}$	D_b^*
0.096	3.00–4.49	2.647	2.655	4.225
0.200	3.00–4.49	1.558	1.554	1.680
0.300	2.00–4.49	1.005	1.018	1.03
0.400	2.00–4.49	0.747	0.746	0.715
0.500	1.50–4.49	0.550	0.545	0.511
0.600	1.00–4.49	0.429	0.416	0.395
0.700	1.00–4.49	0.316	0.311	0.297
0.825	3.00–4.49	0.218	0.218	0.202

[†]Time interval in ps from which the MSD parallel to the pore walls is estimated
[‡]From MSD data
[§]From VACF data

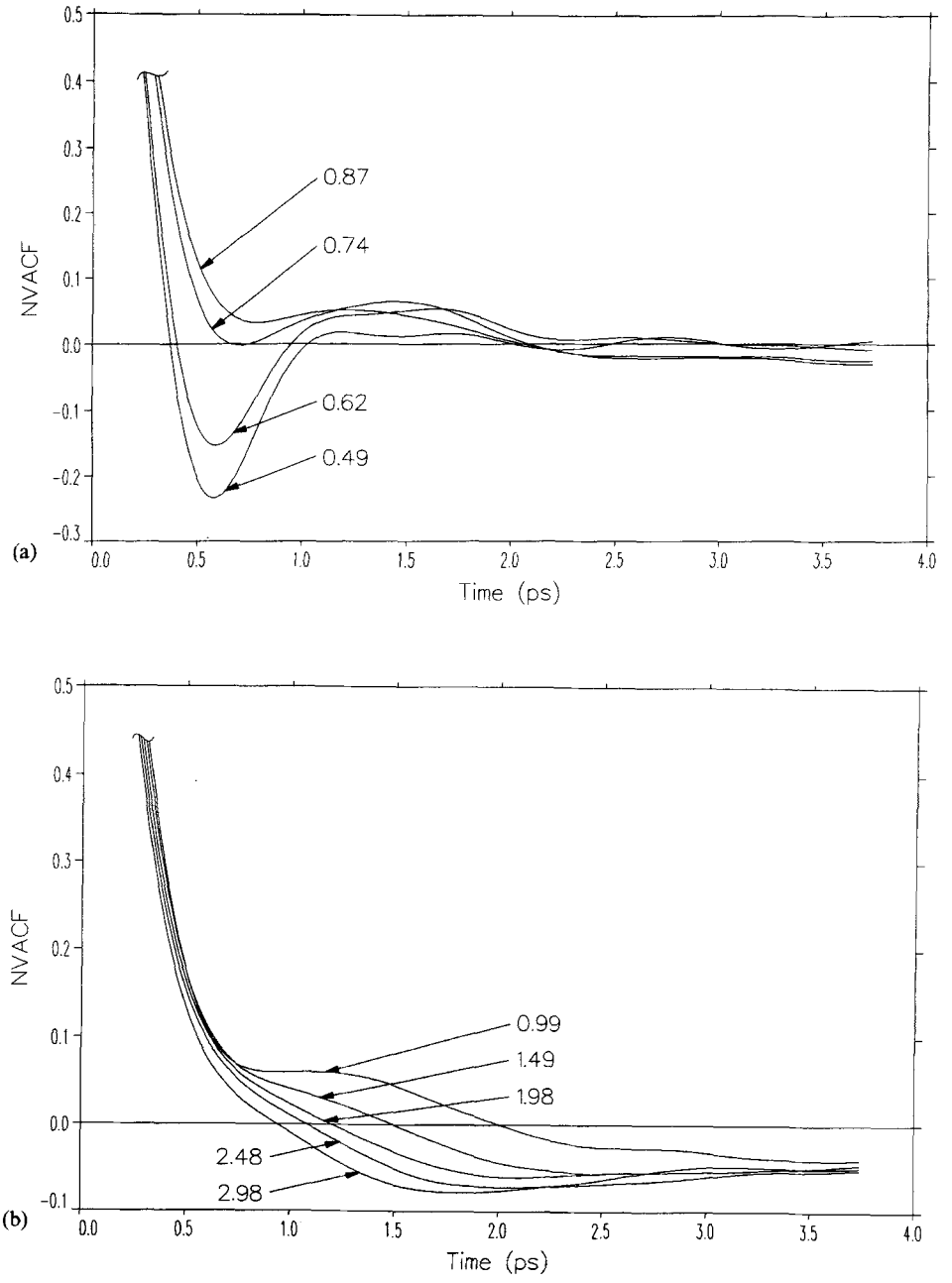

Figure 10 Velocity auto-correlation function perpendicular to the pore walls in a cylindrical pore of radius 2σ at $n_p\sigma^3 = 0.4$ and temperature range kT/σ 0.49–0.87 (Figure 10a) and 0.99–2.98 (Figure 10b).

Table 7 $D_{\parallel}^{*}$ calculated from MSD and VACF data for different densities in a cylindrical pore of radius 2σ. The bulk self-diffusion coefficient D_b^{*} calculated from equation (8) is also presented. The temperature is $kT/\varepsilon = 0.49$

$n_p\sigma^3$	*Range/(ps)*†	$D_{\parallel}^{*\ddagger}$	$D_{\parallel}^{*\S}$	D_b^{*}
0.200	3.50–4.49	0.070	0.069	0.199
0.300	3.00–4.49	0.052	0.052	0.151
0.400	2.00–4.49	0.044	0.044	0.108
0.500	3.00–4.49	0.039	0.039	0.073
0.600	3.50–4.49	0.032	0.0321	0.052
0.700	3.30–4.49	0.028	0.029	0.033
0.825	3.00–4.49	0.024	0.028	0.015

†Time interval in ps from which the MSD parallel to the pore walls is estimated
‡From MSD data
§From VACF data

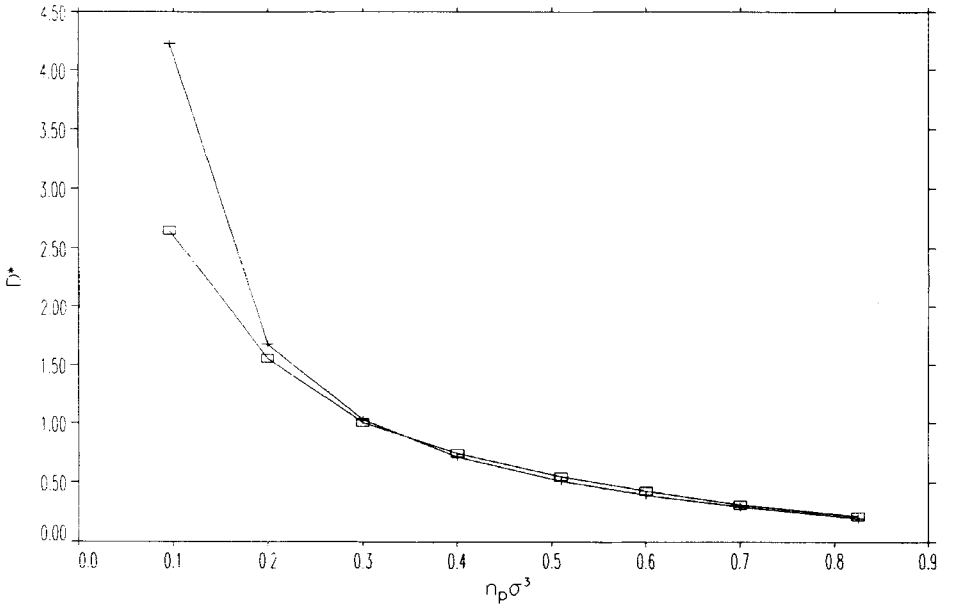

Figure 11 MSD self-diffusion coefficient parallel D_b^{*} (□) to the pore of radius 2σ as a function of density. Also shown is the bulk self-diffusion coefficient $D_{\parallel}^{*}$ (+) calculated from equation (8), at $kT/\varepsilon = 2.98$.

investigation occupying orders of magnitude longer may be necessary to study two phase non-uniform systems. At $kT/\varepsilon = 0.49$ the picture is totally different. $D_{\parallel}^{*}$ being smaller than D_b^{*} at all densities except the highest. $D_{\parallel}^{*}$ here was found to be proportional to $(density)^{-1.38}$ compared with $(density)^{-0.52}$ calculated from equation (8).

3.3 Conclusions

We have presented singlet density profiles for a wide range of temperatures and densities, as well as the temperature and density dependence of the self-diffusion

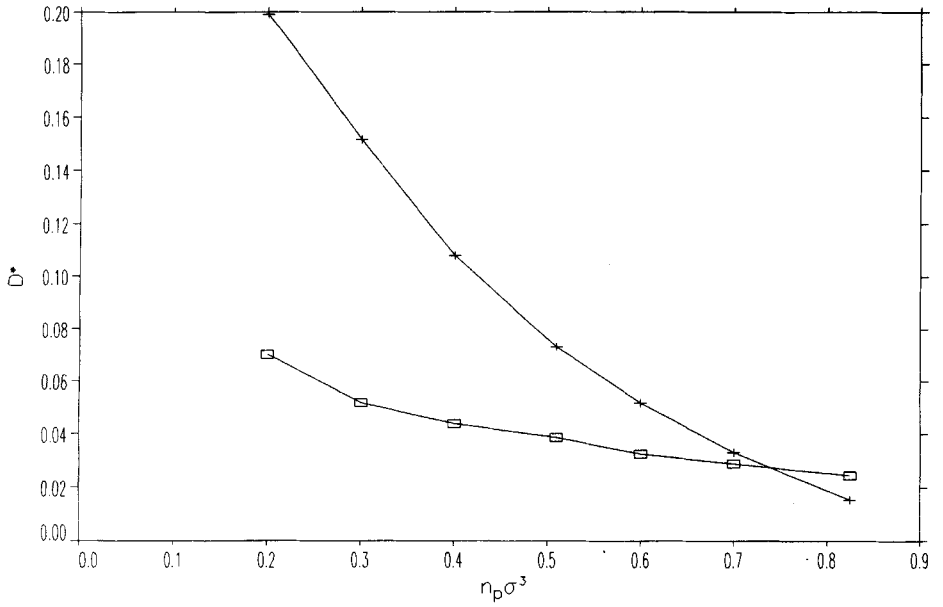

Figure 12 As for Figure 11 at $kT/\varepsilon = 0.49$.

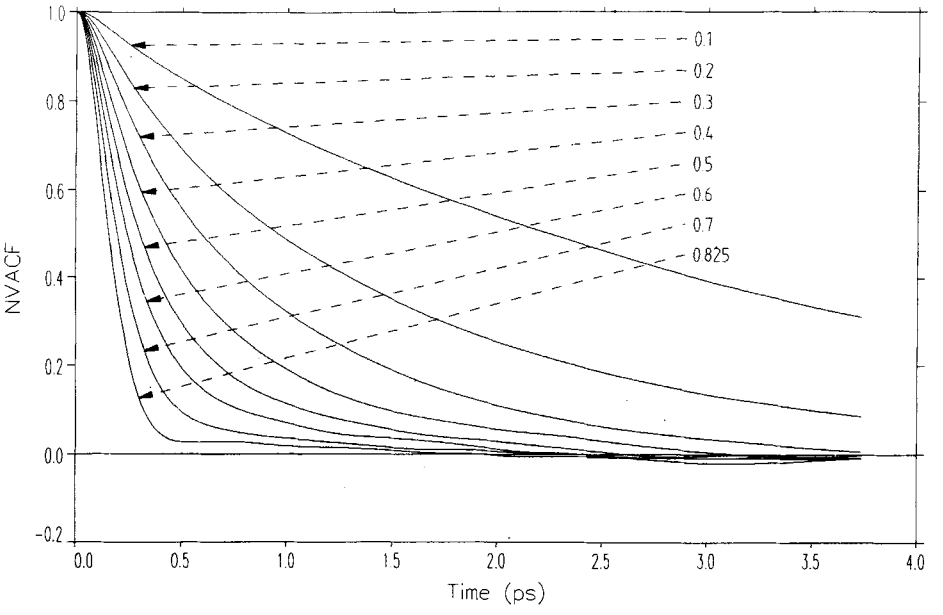

Figure 13 Velocity auto-correlation function parallel to the pore walls in a cylindrical pore of radius 2σ, at temperature $kT/\varepsilon = 2.98$, for a series of densities.

coefficients parallel $D_{\parallel}$ to the pore walls, in a cylindrical pore of radius 2σ. At $n_p\sigma^3 = 0.4$ the curve of $D_{\parallel}$ with kT/ε shows a distinct inflection in the region $0.7 \leqslant kT/\varepsilon \leqslant 0.9$ decreasing to near solid state values at very low temperatures. This behaviour correlates with that observed in the VACF's for motion normal to the wall. The density dependence of $D_{\parallel}$ is rather weaker than inversely proportional at the highest temperature studied ($kT/\varepsilon = 2.98$). At the lowest temperature, $kT/\varepsilon = 0.49$, $D_{\parallel}$ is similar in magnitude to, but less than, the bulk value, D_b.

In the near future we hope to present density profiles in "sphero-cylindrical" pores where spheres are interconnected through cylindrical sections, for a wide range of temperatures and densities. We also intend to investigate the temperature and density dependence of the self-diffusion coefficients parallel and perpendicular to the pore walls inside the pore and compare them with those in cylindrical pores.

Acknowledgements

We wish to thank Mr. Steve Bleazard for his help with computing and Dr. Neville Parsonage for helpful discussions. Many thanks to the British Council for a maintenance grant (to TD) and the University of London Computer Centre for a generous allocation of computer time.

References

[1] V.Y. Antonchenko, V.V. Ilyin, N.N. Makovsky, A.N. Pavlov, and V.P. Sokhan "On the nature of disjoining pressure oscillations in fluid films". *Molecular Physics*, **52(2):** 345–355 (1984).
[2] G. Subramanian and H.T. Davis "Molecular dynamics of a hard sphere fluid in small pores." *Molecular Physics*, **38(4):** 1061–1066 (1979).
[3] J.J. Magda, M. Tirrell, and H.T. Davis "Molecular dynamics of narrow, liquid-filled pores." *J. Chem. Phys.*, **83a(4):** 1888–1901 (1985).
[4] S. Das Sarma, K. E. Kohr, S.M. Paik, and T.R. Kirkpatrick "Molecular dynamics study of self-diffusion in a thin film Lennard-Jones system." *Chem. Phys. Let.*, **120(1):** 97–100 (1985).
[5] U. Heinbuch and J. Fischer "Liquid argon in a cylindrical carbon pore; Molecular Dynamics and Born-Green-Yvon results." *Chem. Phys. Let.*, **135(6)**: 587–590 (1987).
[6] B.K. Peterson and K.E. Gubbins "Phase transitions in a cylindrical pore. Grand Canonical Monte Carlo, Mean field theory and the Kelvin equation." *Molecular Physics*, **62(1):** 215–226 (1987).
[7] G.S. Heffelfinger, F. van Swol, and K.E. Gubbins "Liquid-vapour coexistence in a cylindrical pore." *Molecular Physics*, **61(6):** 1381–1390 (1987).
[8] B.K. Peterson, K.E. Gubbins, *et al.* "Lennard-Jones fluids in cylindrical pores: Nonlocal theory and computer simulation. "*J. Chem. Phys.*, **88:** 6487–6500 (1988)
[9] S.H. Suh and J.M.D. MacElroy "Molecular dynamics simulation of hindered diffusion in microcapillaries." *Molecular Physics*, **58(3):** 445–473 (1986).
[10] A. Panagiotopoulos. "Adsorption and capillary condensation of fluids in cylindrical pores by Monte Carlo simulation in the Gibbs ensemble." *Molecular Physics*, **62(3):** 701–719 (1987).
[11] J.M.D. MacElroy and S.H. Suh "Simulation studies of a Lennard-Jones liquid in micropores." *Molecular Simulation*, **2:** 313–351 (1989).
[12] A. Rahman "Correlations in the motion of atoms in liquid argon." *Phys. Rev.*, **136:** 405–411 (1964).
[13] B.J. Alder and T.E. Wainwright "Velocity autocorrelation for hard spheres." *Phys. Rev. Letters*, **18:** 988–991 (1967).
[14] B.J. Alder and T.E. Wainwright "Decay of the Velocity Autocorrelation Function." *Phys. Rev. A*, **1:** 18–21 (1969).
[15] B.J. Alder, D.M. Gass, and T.E. Wainwright "Studies in molecular dynamics. VIII. The transport coefficients for a hard-sphere fluid." *J. Chem. Phys.*, **53(10)** 3813–3826 (1970).
[16] D. Levesque and L. Verlet "Computer 'experiments' on classical fluids. III. Time dependent self-correlation functions." , *Phys. Rev. A*, **2:** 2514–2528 (1970).
[17] I.K. Snook and D. Henderson "Monte Carlo study of a hard-sphere fluid near a hard wall." *J. Chem. Phys.*, **68:** 2134–2139 (1978).
[18] I.K. Snook and W. van Megen "Solvation forces in simple dense fluids." *J. Chem. Phys.*, **72:** 2907–2913 (1980).

[19] J.N. Cape "Molecular dynamics study of a dense fluid at a hard wall." *J. Soc., Faraday Trans.* **2, 78:** 317–326 (1982).
[20] J.R. Henderson and F. van Swol "On the interface between a fluid and a planar wall. Theory and simulations of a hard sphere fluid at a hard wall." *Molecular Physics,* **58(4):** 991–1010 (1984).
[21] G.B. Woods, A.Z. Panagiotopoulos, and J.S. Rowlinson "Adsorption of fluids in model zeolite cavities." *Molecular Physics,* **63(1):** 49–63 (1988).
[22] J.L. Soto and A.L. Myers "Monte Carlo studies of adsorption in molecular sieves." *Molecular Physics,* **42(4):** 971–983 (1981).
[23] R.W. Hockney "The potential calculation and some applications." *Methods Comput. Phys.,* **9:** 136–211 (1956).
[24] D. Potter. *Computational Physics.* Wiley, New York, (1972).
[25] M.P. Allen and D.J. Tildesley *Computer Simulation of Liquids.* Oxford University Press, (1987).
[26] D.M. Heyes "Self-diffusion and shear viscosity of simple fluids." *J. Chem., Faraday Trans.* **2, 79:** 1741–1747 (1983).
[27] T. Demi *A simulation study of adsorption and transport in model pores.* PhD thesis, Imperial College of Science, Technology and Medicine (1989).